Losing the shock wave front profile due to interaction with turbulence

Gaku Fukushima, Jiaxi Wei, Shingo Ogawa, Jun Hagiwara, Yusuke Nakamura and Akihiro Sasoh

Department of Aerospace Engineering, Nagoya University, Furo-cho, Chikusa, Nagoya 464-8603, Japan

E-mail: fukushima.gaku@a.mbox.nagoya-u.ac.jp

Abstract. In this study, losing the shock wave profiles under interactions with grid turbulence was investigated experimentally and theoretically. We demonstrated that the shock wave contrast on side-view schlieren images gradually decreased to an undetectable level. This shock wave "vanishment" occurred at a low shock Mach number with a high turbulent Mach number. With a relatively strong shock wave, the contrast of the shock wave remained detectable although the shock wave profile region was expanded. To understand the shock wave vanishment phenomenon during interaction with turbulence, we established a shock wave vanishment model based on the solution of a one-dimensional interaction between a shock wave and forward induced flow. The criterion of the occurrence of local vanishment of the shock wave was derived as $M_\mathrm{t} \geq (M_\mathrm{s}^2 - 1)/M_\mathrm{s}$, where M_t is the turbulent Mach number and M_s is the shock Mach number. The proposed shock vanishment model involves the effect of the interaction length and the shock wave recovery characteristics. The derived model explains the disappearance of weak shock wave during turbulence with an interaction length of 10 times the order of the integral scale of the turbulence, as observed in the experiment.

Keywords: Shock waves, turbulence, Shock−turbulence interaction

1. Introduction

The interaction of a shock wave with turbulence causes a drastic mutual modulation of both characteristics (Andreopoulos et al 2000). Shock–turbulence interactions occur in engineering applications such as supersonic and hypersonic propulsion systems and inertial-confinement fusion. Supernova explosions and volcanic eruptions have deep relationships with such interactions. Many investigations of the behavior of shock waves and turbulence during interactions have been conducted via theoretical, numerical, and experimental methods. The primary system studied is that of interaction between a normal shock wave whose characteristics do not change during propagation and isotropic turbulence. In this system, the modulations of a shock wave and turbulence have been studied using numerical and experimental methods.

Direct numerical simulation (DNS) has been used to investigate the interaction of a normal shock with isotropic turbulence (Lee et al 1993, Larsson and Lele 2009, Larsson et al 2013, Ryu and Livescu 2014, Livescu and Ryu 2016, Tian et al 2017, Tanaka et al 2018 and 2020, Chen and Donzis 2019). In some DNS simulations, a turbulent upstream flow interacts with a spatially fixed shock wave in the shock wave fixed-coordinate system. Donzis (2012) derived the criterion for the initial appearance of a hole on the shock wave (broken shock regime) as $M_\mathrm{t} \geq 0.6(M-1)$, where M_t is the turbulent Mach number, and M is the mean upstream flow Mach number. Thereafter, Larsson et al (2013) and Chen and Donzis (2019) confirmed this theory's consistency with the DNS results. Furthermore, Chen and Donzis (2019) reported that a shock wave widely loses its discontinuity in the case of strong turbulence, known as the "vanished" regime of the interaction. However, Deviating from the real phenomena, in these DNSs, the boundary condition proposed by Lele (1992) was applied to perform the simulation. Such numerical simulations yielded results in a "steady" state determined by a "fixed" shock wave strength and upstream flow condition. In real situations, a shock waves are often generated by the dynamics of driving sources. The series of behaviors of a shock wave entering and propagating through turbulence involves an "unsteady" modulation. Some DNSs adopted such a system (Tanaka et al 2018 and 2020), but investigations of unsteady shock wave behavior are insufficient.

Although experimental studies on shock–turbulence interactions have been conducted in various systems (Lipkens and Blackstock 1998, Kim et al 2010, Sasoh et al 2014, Tamba et al 2016, Kitamura et al 2017, Inokuma et al 2017 and 2019), it has been challenging to realize the interaction between a normal shock wave and isotropic turbulence. Dosanjh (1956), Honkan and Andreopoulos (1992), Honkan et al (1994), Xanthos et al (2002), and Agui et al (2005) used shock tubes to induce interactions of normal shock wave reflected from the end walls with grid turbulence. However, in a typical shock tube with a single driver and driven section, it is difficult to conduct parametric surveys. Our research group previously developed a counter-driver shock tube (CD-ST) with an additional driver section incorporated with a typical shock tube to overcome these experimental difficulties (Tamba et al 2015). This experimental ap-

paratus enables the independent establishment of specific shock and turbulent Mach numbers and interaction lengths. In our previous works (Tamba et al 2019, Fukushima et al 2021), we observed shock wave deformation with grid turbulence as the interaction length increased. However, the "vanished" state, as demonstrated in DNS research, has not been investigated experimentally. The objective of this study is to demonstrate the shock wave vanishment and improve the physical understanding of this phenomenon.

2. Experimental setup and condition

The experiment was conducted using a CD-ST. The CD-ST is a diaphragm-type shock tube with two driver sections at both ends of the driven sections. Its total length is approximately 14 m; it has a square cross-section measuring 120 mm $\times$ 120 mm. The operation timings of the two drivers are actively controlled under a set driver. Since the pressures of the driver sections are controlled independently, we can independently control the Mach numbers of the shock waves generated in the driven section. Figure 1 shows an example of an x (space)–t (time) diagram of the CD-ST operation. Each driver generated left- and right-incident shock waves (represented as L-iSW and R-iSW, respectively). Under some conditions, as described later, we weakened the L-iSW using punched stainless steel sheets installed at $x = 1.0$ m. R-iSW passed through a square grid and became a grid-past shock wave (i.e., R-gSW). The square grid containing 5 mm $\times$ 5 mm square pillars with a mesh size of 25 mm was installed at $x = 5.0$ m, as shown in Figure 1. A uniform flow behind R-iSW was transmitted to the grid turbulence beyond the square grid. After the collision of L-iSW and R-gSW, the transmitted shock waves, L-tSW, and R-tSW propagated in the directions shown. At a certain point, L-tSW entered and interacted with the grid turbulence. We defined the interaction length, L_{i}, as the distance from the shock waves to the head of the grid turbulence. The value of L_{i} was controlled by the time difference τ of the operation of each driver. We visualized the shock wave propagating through the grid turbulence by a schlieren method. The visualization system consisted of a high-speed camera (Phantom v1211, Vision Research Inc.; 256 $\times$ 256 pixels, 100 kfps) and synchronized pulse diode laser (CAVILUX Smart, Cavitar Ltd.; wavelength 640 nm, pulse duration 10 ns). This system visualized the shock wave at a pair of BK7 windows (effective diameter of 110mm) installed on the sidewall at 450 mm downstream of the square grid. The optical path from the test section to the high-speed camera was approximately 20 m to facilitate the capture of weak density changes with high sensitivity. Additional details on the facility principle and instrumentation can be found in our previous papers (Tamba et al 2015 and 2019, Fukushima et al 2021).

The main role of the right driver was the generation of the grid turbulence behind R-gSW. In this experiment, we used a single condition of the grid turbulence. Thus, the right-driver and the driven sections' initial pressure conditions were kept equal to those under the CD-ST operation. The initially filled gas in the right driver was a mixture of

He and atmospheric air supplied from a compressor through a dryer. The fill pressure ratio was He:air = 9:1. Air was used as the driven gas. The initial pressure condition of the right driver and that in the driven section were $p_{4R} = 128.3$ kPa and $p_1 = 12.3$ kPa, respectively. The shock wave velocity was measured by the time-of-flight principle. By dividing the shock wave velocity by the speed of sound in the gas in the driven section, the shock Mach numbers of R-iSW and R-gSW were calculated as $M_{s,\text{R-iSW}} = 1.82$ and $M_{s,\text{R-gSW}} = 1.76$, respectively. Here, we assumed that the gas in the driven section was calorically perfect such that the specific heat capacity is a constant value ($\gamma = 1.4$). The velocity of the grid turbulence's mainstream flow was approximately 340 m/s, as calculated by the Rankine–Hugoniot relations. The left driver conditions primarily determined the shock Mach number of the interacting shock wave, i.e., $M_{s,\text{L-tSW}}$. In this research, we set the left driver pressure either to $p_{4L} = 18.3$ or 20.3 kPa depending on the condition. Moreover, two types of punched stainless steel sheets were used to change the shock Mach number. Type A comprised 16 punched stainless steel sheets of 0.8-mm thickness, 1-mm hole diameter, and a blocking ratio of 82.5%. Type B comprised three punched stainless steel sheets of 1-mm thickness, 2-mm hole diameter, and a blocking ratio of 64%. When p_{4L} was 18.3 kPa, we obtained $M_{s,L-tSW} = 1.006, 1.034$, and 1.046 using types A and B punched stainless steel sheets and without sheets, respectively. When p_{4L} was 20.3 kPa, we obtained $M_{s,\text{L-tSW}} = 1.013$ using type A punched stainless steel sheets. Here, the shock Mach number of the left-transmitted shock wave, $M_{s,\text{L-tSW}}$, was calculated with the solution from the head-on collision of L-iSW and R-gSW.

3. Experimental results

Under the conditions applied in this study, measurement of the grid turbulence characteristics could not be performed because the hot-wire probe was broken by finely ruptured cellophane debris. Therefore, the turbulent Mach number was estimated through a linear extrapolation using the obtained relation between the mean flow velocity and the turbulent Mach number reported in the previous study by Fukushima et al (2021). The near-linear relationship between the mainstream-flow Mach number of the grid turbulence and the turbulent Mach number can be seen in the measurement of grid turbulence generated in a shock tube in the range from 0.3 to 0.7 for a constant mesh size (Briassulius et al 1998). We apply this linear relationship to our facility. With a mean grid turbulence velocity of 340 m/s and a flow Mach number of 0.72 (calculated by the Rankine-Hugoniot equations in a perfect gas), the representative value of the turbulent Mach number was $\widetilde{M_t} = 0.025$ (the tilde represents the value at the center of the visualizing window located at 450 mm downstream of the grid). Because the data used to estimate $\widetilde{M_t}$ involved a standard deviation of approximately 10%, the estimated $\widetilde{M_t}$ could contain the same extent of error. As the generated grid turbulence was not supersonic flow, strong disturbances such as shocklets could not be confirmed in the schlieren images. Pressure oscillation in the grid turbulence, which was induced mainly in the initial diaphragm rupture processes, was 1.7% of the absolute pressure in the

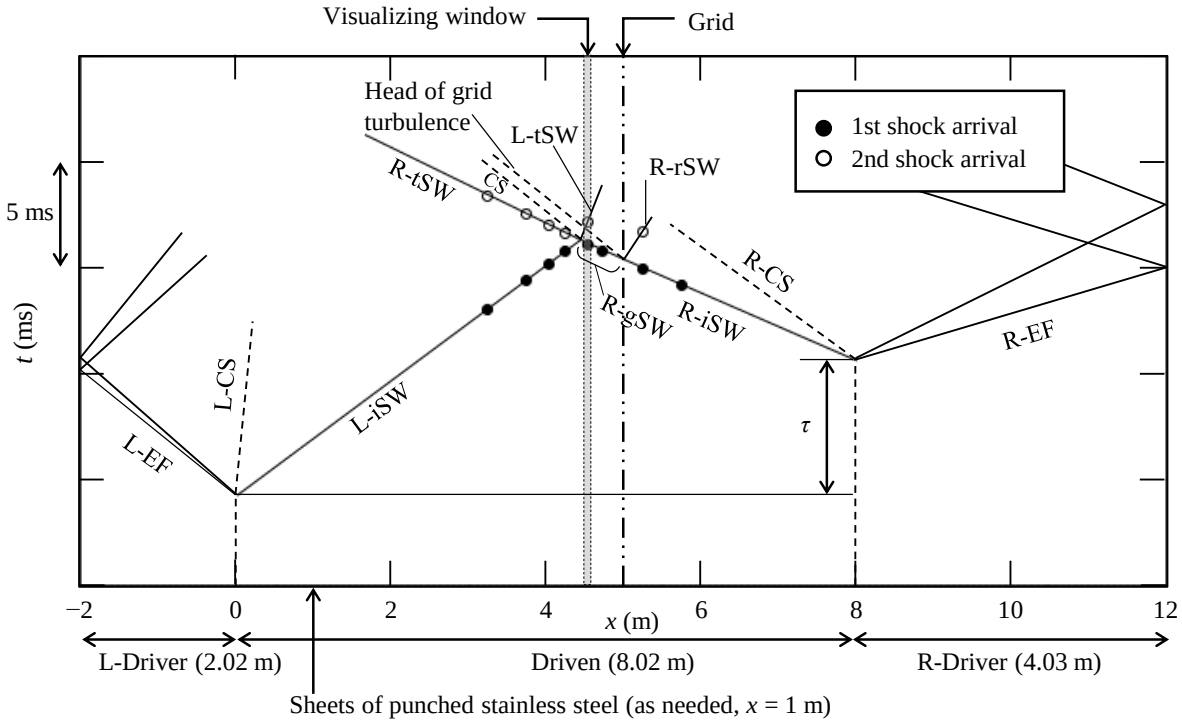

Figure 1: Example of an x–t diagram of the CD-ST operation: $p_{4\mathrm{L}} = 20.8$ kPa, $p_1 = 12.8$ kPa, and $p_{4\mathrm{R}} = 128.3$ kPa; SW, shock wave; EF, expansion fan; CS, contact surface.

grid turbulence based on pressure measurement by a flush-mounted pressure sensor on the inner wall of the shock tube. This pressure oscillation caused a 1.3% change in the speed of sound.

The schlieren visualization results of a shock wave moving from left to right against the grid turbulence blowing from right to left are shown in Figure 2. To enhance the signal-to-noise ratios in the images, all images shown in this paper are differential images formed by subtracting the quiescent-state image before shock tube operation from the rough image (Kim er al 2010). In Figure 2, the shock tube center measuring approximately 86 mm range is extracted. The positive and negative values of L_i correspond to the interaction lengths during and before the interaction, respectively. The image sequences presented in each row were extracted from the same CD-ST operations. The image sequence in the lower row corresponds to the trial in the long-interaction-length case. In the interaction of the weakest-shock wave case of $M_{\mathrm{s,L\text{-}tSW}} = 1.006$ (Figure 2 (a)), the shock wave was perfectly planar before interacting with the grid turbulence ($L_\mathrm{i} < 0$). After the interaction, the shock wave contrast on the visualized image gradually diminished with increases in the interaction length. At $L_\mathrm{i} = 200$ mm, the shock wave profile could not be detected on the schlieren images. Eventually, the contrast level of the shock wave became equivalent to the density changes caused by the grid turbulence. In the case of $M_{\mathrm{s,L\text{-}tSW}} = 1.013$, a similar result was

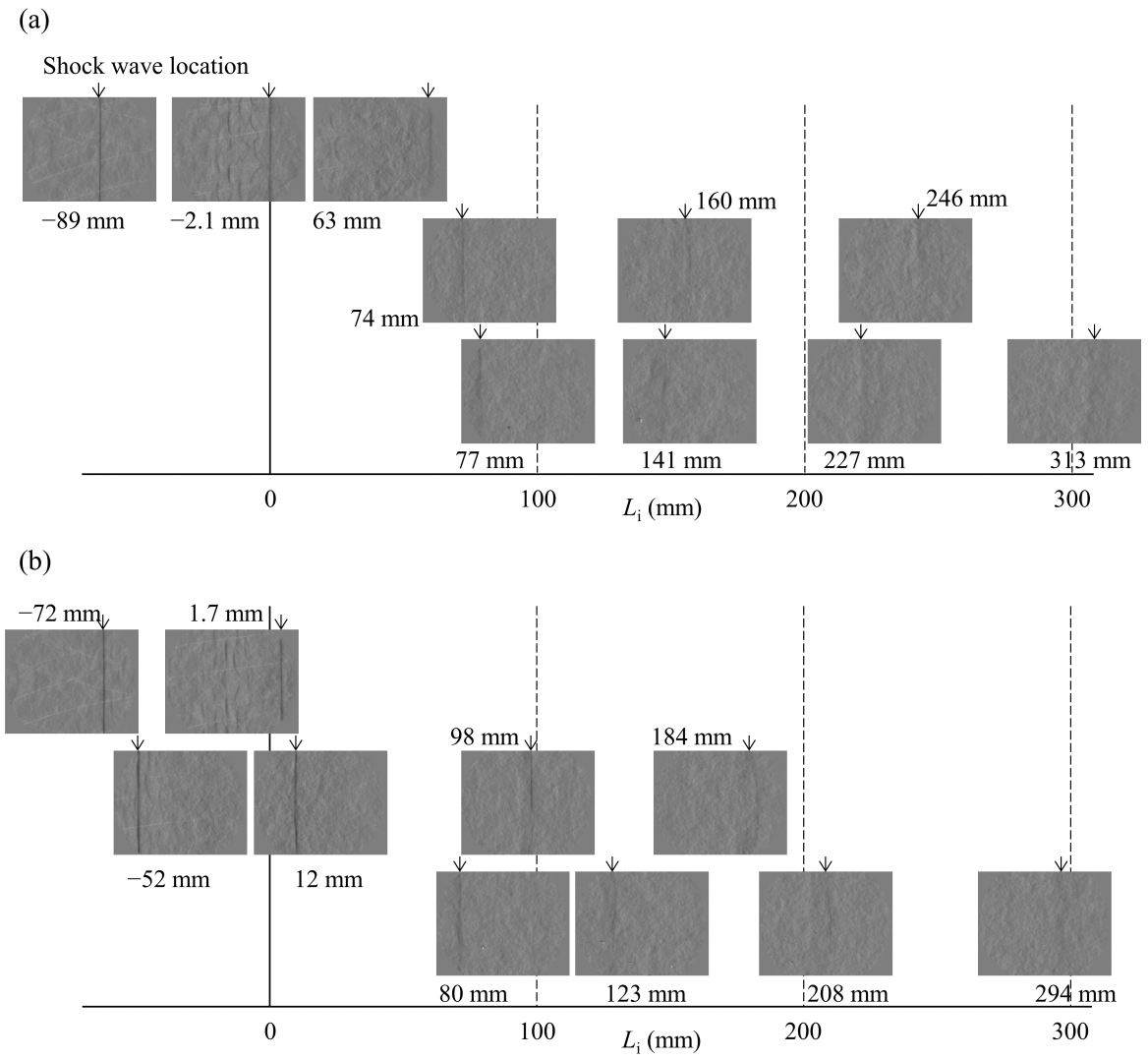

Figure 2 (a) and (b)

observed. When L_i exceeded 300 mm, we could not observe the shock wave profile. Because the schlieren visualization integrates information from a spanwise direction, a sharp line is obviously apparent if the shock wave remains locally. Therefore, the shock wave lost its discontinuous profile because of interactions with the grid turbulence. Regarding this shock wave behavior, Chen and Donzis (2019) recently reported the "vanished" regime of the interaction, where the upstream and downstream cannot be identified unambiguously from DNS results. A similar result was observed in our experiment. However, we found novel insight from the experiment of moving the shock wave: the gradually vanished with the increase in interaction length. In contrast to the case of the weak shock wave, the relatively strong shock waves with $M_{\mathrm{s,L\text{-}tSW}} = 1.034$ and 1.046 were largely deformed and with expansions in the side projected areas with the grid turbulence, but the shock wave profiles remained even under the long-interaction-length cases, i.e., $L_\mathrm{i} = 200$ mm. Schlieren-visualized movies of these experiments are

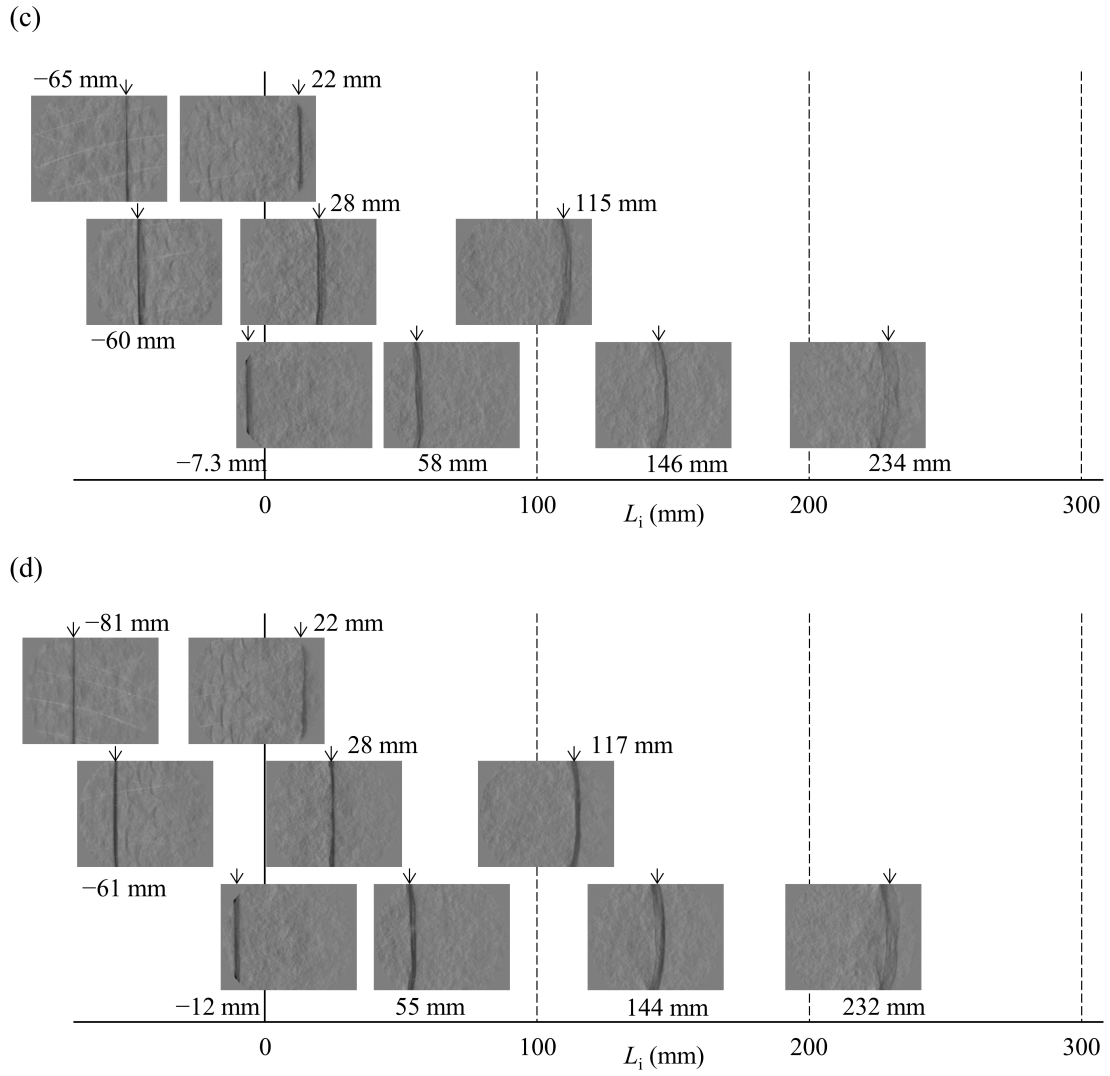

Figure 2: Schlieren images of the shock wave propagating through the grid turbulence. Arrows indicate the trajectory of the shock wave propagating at a constant velocity: (a) $M_{\mathrm{s,L\text{-}tSW}} = 1.006$, (b) $M_{\mathrm{s,L\text{-}tSW}} = 1.013$, (c) $M_{\mathrm{s,L\text{-}tSW}} = 1.034$, and (d) $M_{\mathrm{s,L\text{-}tSW}} = 1.046$.

presented in the supplementary data.

4. Modeling of shock wave vanishment by a one-dimensional unsteady compression theory and discussion

To physically interpret the shock wave profile vanishment during turbulence interaction, we consider the shock wave modulation based on a one-dimensional (1D) unsteady compression problem called the Riemann problem (Shapiro 1953, Liepmann and Roshko 1957, Glass and Sislian 1994, Sasoh 2020). As shown in Figure 3, the most fundamental subsequent situation is considered, i.e., a shock wave propagating in the quiescent state

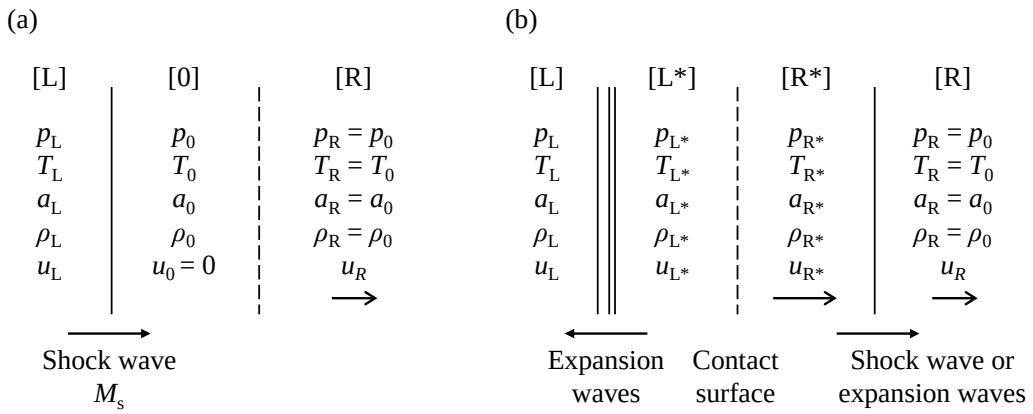

Figure 3: Schematics of a 1D shock wave−forward-induced-flow interaction: (a) before interaction, (b) after interaction.

with the shock Mach number of M_s interacts with a forward induced flow. The states 0, L, and R correspond to the quiescent state, the area behind the incident shock wave, and the forward induced flow, respectively. Here, the states 0 and R are assumed to have the same pressure. In addition, we assume that the proprieties of the states 0 and R discontinuously change. The gas of all states is calorically perfect: the specific heat ratio is constant ($\gamma = 1.4$). When the induced shock wave enters state R, new right- and left-running waves are generated. The states after passing the left- and right-running waves are L* and R*, respectively. The contact surface separates states L* and R*. A schematic of the u (velocity)–p (pressure) diagram of the interaction is shown in Figure 4. When the induced velocity direction has the same direction as the shock wave propagation, the increase in pressure by the right-running wave (curve R $\rightarrow$ R*) becomes smaller than that by the incident (curve 0 $\rightarrow$ L). In this case, left-running expansion waves are generated.

Here, we derive the condition where the pressure increase induced by a right-running wave is equal to zero. In this case, the incident shock wave transits to a sound wave through an interaction with the forward induced flow. When quantity changes do not occur with the right-running wave, the following equations are obtained:

$$\begin{aligned} p_{\mathrm{R}*} &= p_{\mathrm{R}}, \\ u_{\mathrm{R}*} &= u_{\mathrm{R}}. \end{aligned} \tag{1}$$

Because the left-running wave is composed of expansion waves, as shown in Figure 4, the following isentropic equation between states L and L* is obtained:

$$\frac{u_{\mathrm{L}*} - u_{\mathrm{L}}}{a_{\mathrm{L}}} = \frac{2}{\gamma - 1}\left[1 - \left(\frac{p_{\mathrm{L}*}}{p_{\mathrm{L}}}\right)^{\frac{\gamma-1}{2\gamma}}\right]. \tag{2}$$

Pressure and velocity are equal across the contact surface between states L* and R*.

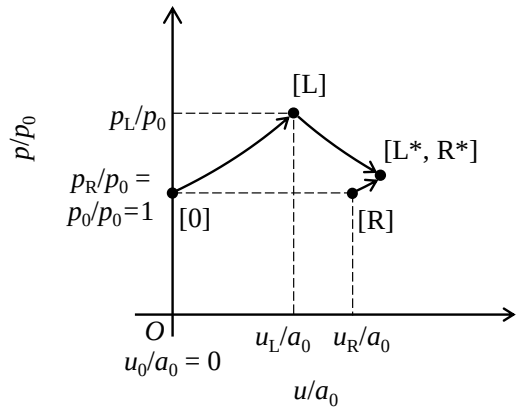

Figure 4: Schematic of u–p diagram

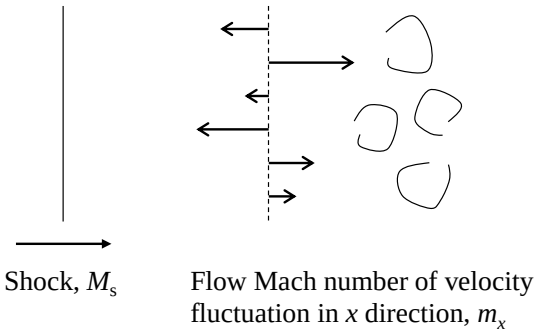

Figure 5: Schematic of the x-element in a shock wave–turbulence interaction

Accordingly, we obtain:

$$\begin{aligned} p_{\mathrm{L}*} &= p_{\mathrm{R}*}, \\ u_{\mathrm{L}*} &= u_{\mathrm{R}*}. \end{aligned} \tag{3}$$

By deleting the variables of states L* and R* using (1)–(3) and expressing the variable state L by the incident shock Mach number M_s, we obtain the ratio of the velocity of the forward induced flow u_R to the velocity behind the incident shock wave u_L as a function of M_s, as follow:

$$\frac{u_\mathrm{R}}{u_\mathrm{L}} = 1 + \frac{\left(2\gamma M_\mathrm{s}^2 - \gamma + 1\right)^{\frac{1}{2}} \left[\left(\gamma - 1\right) M_\mathrm{s}^2 + 2\right]^{\frac{1}{2}}}{\left(\gamma - 1\right)\left(M_\mathrm{s}^2 - 1\right)} \left[1 - \left(\frac{2\gamma M_\mathrm{s}^2 - \gamma + 1}{\gamma + 1}\right)^{-\frac{\gamma-1}{2\gamma}}\right]. \tag{4}$$

The right side of (4) becomes 2 at the limit of the weak shock wave of $M_\mathrm{s} \to 1$, and the relationship $|u_\mathrm{R}/u_\mathrm{L} - 2| < 0.005$ holds for values of M_s from 1 to 2. Therefore, we can regard $u_\mathrm{R}/u_\mathrm{L} = 2$ for the weak shock wave. The values of u_R and u_L can be expressed

as dimensionless Mach numbers as follows:

$$\begin{aligned} \frac{u_{\mathrm{R}}}{a_0} &= M_{\mathrm{R}}, \\ \frac{u_{\mathrm{L}}}{a_0} &= \frac{2}{\gamma+1}\left(\frac{{M_{\mathrm{s}}}^2-1}{M_{\mathrm{s}}}\right). \end{aligned} \tag{5}$$

where M_{R} is the Mach number of forward induced flow. Using (5), we can express the relationship $u_{\mathrm{R}}/u_{\mathrm{L}} = 2$ with dimensionless Mach numbers. The following inequality gives the relationship of the shock wave transition to a sound wave or expansion wave when the shock wave interacts with the forward induced flow in a 1D system.

$$M_{\mathrm{R}} \geq \frac{4}{\gamma+1}\frac{{M_{\mathrm{s}}}^2-1}{M_{\mathrm{s}}}. \tag{6}$$

Next, the shock wave state interacting with the turbulence is considered using a similar analysis proposed by Donzis (2012). In his analysis, the possibility of having a local Mach number less than unity in some locations showed good agreement with that of the appearance of holes in the shock wave, as confirmed by DNS results (Larsson et al 2013, Chen and Donzis 2019). In this research, the interaction between moving shock waves with planar distributed velocity fluctuations is considered, as shown in Figure 5. Thus, we calculate the probability of having a local flow Mach number satisfying (6) in some location as the probability of the local vanishment of the shock wave. Here, it is assumed that only the velocity is disturbed. In addition, only the elements facing the shock wave (x-direction) are considered. The turbulence velocity fluctuation is assumed to obey a Gaussian distribution, which is considered a good approximation (Monin and Yaglom 1975). In the location where the Mach number of the "local" turbulence velocity fluctuation mx exceeds the flow Mach number M_{R}, thus satisfying (6), the incident shock wave locally vanishes. The probability of the existence of a local flow satisfying (6) in the turbulence is defined as $P\left(m_x > M_{\mathrm{R}}\right)$, where $P()$ is a function of probability of satisfying inequality in (). Under the assumption of a Gaussian-distribution velocity fluctuation, the value of $P\left(m_x > M_{\mathrm{R}}\right)$ can be statistically expressed as a simple form using the error function erf() as $P\left(m_x > M_{\mathrm{R}}\right) = 1 - 1/2\left\{1 + \mathrm{erf}\left[M_{\mathrm{R}}/\left(\sqrt{2/3}M_{\mathrm{t}}\right)\right]\right\}$. Here, regarding the turbulent Mach number, $M_{\mathrm{t}} = \sqrt{3}u'_x/a_t$ is applied because the turbulence is assumed to be isotropic, where u'_x is the x component of the velocity fluctuation, and at is the speed of sound of the turbulence. Here, we define the probability of local shock wave vanishment for one interaction of the shock wave with a fluctuating-velocity plane as P_1. By substituting (6), we can write P_1 as a function of the shock Mach number M_{s} and the turbulent Mach number M_{t}:

$$P_1 = P\left(m_x > M_{\mathrm{R}}\right) = 1 - \frac{1}{2}\left[1 + \mathrm{erf}\left(\frac{\frac{M_{\mathrm{s}}^2-1}{M_{\mathrm{s}}}}{\sqrt{\frac{2}{3}}\frac{\gamma+1}{4}M_{\mathrm{t}}}\right)\right]. \tag{7}$$

Figure 6 shows a plot of Eq(7) as a function of $M_{\mathrm{s}}M_{\mathrm{t}}/\left({M_{\mathrm{s}}}^2-1\right)$. The four plotted points correspond to the experimental conditions considered in this study. The value of $P\left(m_x > M_{\mathrm{R}}\right)$ is almost 0 in $M_{\mathrm{s}}M_{\mathrm{t}}/\left({M_{\mathrm{s}}}^2-1\right) < 1$. At $M_{\mathrm{s}}M_{\mathrm{t}}/\left({M_{\mathrm{s}}}^2-1\right) = 1$,

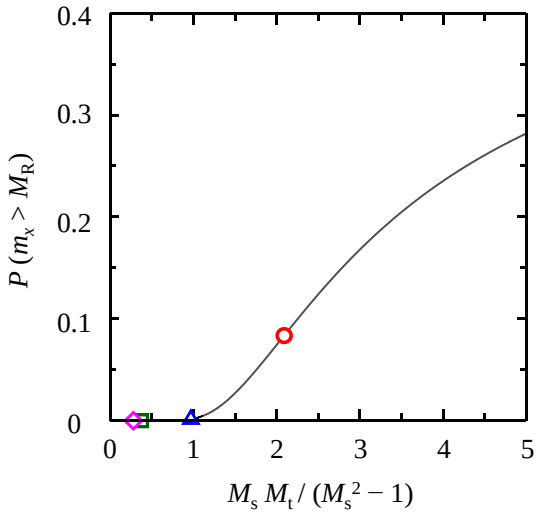

Figure 6: Shock vanishment probability after one interaction $P\,(m_x > M_\mathrm{R})$ as a function of $M_\mathrm{s}M_\mathrm{t}/\left({M_\mathrm{s}}^2 - 1\right)$. Plots correspond to $M_\mathrm{s,L\text{-}tSW} = 1.006$ (circle), $M_\mathrm{s,L\text{-}tSW} = 1.013$ (triangle), $M_\mathrm{s,L\text{-}tSW} = 1.034$ (square), and $M_\mathrm{s,L\text{-}tSW} = 1.046$ (diamond), respectively. $\widetilde{M}_\mathrm{t} = 0.025$ under all conditions.

the value of $P\,(m_x > M_\mathrm{R})$ is 0.002, and $P\,(m_x > M_\mathrm{R})$ starts to increase with $M_\mathrm{s}M_\mathrm{t}/\left({M_\mathrm{s}}^2 - 1\right) = 1$ as the threshold value. Therefore, we obtain the following inequality as a condition for the appearance of shock wave local vanishment with one interaction in the fluctuating-velocity plane:

$$M_\mathrm{t} \geq \frac{{M_\mathrm{s}}^2 - 1}{M_\mathrm{s}}. \tag{8}$$

Equation (8) gives the probability of local shock wave vanishment for one interaction of the shock wave with a fluctuating-velocity plane. However, such a case is rare in real situations, in which the shock waves repetitively interact with velocity fluctuations during propagation through turbulent regions of certain volumes. Thus, hereafter, we consider the repetitive interaction effect on the vanishment of weak shock wave. In a repetitive interaction with velocity fluctuations, the shock wave constantly experiences modulation during propagation. Because quantity change caused by weak shock waves can be regarded as isentropic (Shapiro 1953, Liepmann and Roshko 1957, Glass and Sislian 1994, Sasoh 2020), the flow Mach number that causes the vanishment of the shock wave is determined only by the shock Mach number of the incident shock wave: the shock wave vanishment condition of (6) does not change in the interaction. Therefore, we can consider that the shock wave locally vanishes when it meets the flow satisfying (6) during propagation in turbulence.

In addition, we must consider the shock wave behavior after vanishment. We discuss this behavior in this paragraph. After the shock wave is locally vanished, compression waves are formed by multidimensional effects surrounding the vanished

area. Therefore, the recovery state of the shock wave from the compression waves is important in modeling the behavior of the shock wave propagating through turbulence. We quantitatively analyze the shock wave reformation under experimental conditions similar to those in a 1D analysis presented by Sasoh 2020. Here, we consider the bundle of compression waves propagating from right to left in which initially ($t = 0$) its leading head is located at $x = x_{\mathrm{a}}$ and the tail is at $x = x_{\mathrm{b}}$; see Figure 7. We assume that the pressure variation between x_{a} and x_{b} is continuous. The thickness of the bundle is $\Delta x = x_{\mathrm{a}} - x_{\mathrm{b}}$. Because the local velocity of the characteristic increases with increases in pressure, the tail compression wave gradually catches up with the head compression wave at $t = t_{\mathrm{s}}$, thus forming a shock wave. We define the shock formation location as $x = x_{\mathrm{s}}$, and the shock formation distance L is defined as $L = x_{\mathrm{s}} - x_{\mathrm{a}}$. The time of shock formation t_{s} is written using the velocities of characteristics $c_{+,\,\mathrm{a}}$ and $c_{+,\,\mathrm{b}}$ as follows:

$$t_{\mathrm{s}} = \frac{L}{c_{+,\,\mathrm{a}}} = \frac{L + \Delta x}{c_{+,\,\mathrm{b}}}. \tag{9}$$

This equation can be rewritten as

$$\frac{L}{\Delta x} = \frac{c_{+,\,\mathrm{a}}}{c_{+,\,\mathrm{b}} - c_{+,\,\mathrm{a}}}, \tag{10}$$

where $c_{+,\,\mathrm{a}}$ and $c_{+,\,\mathrm{b}}$ are written using the flow velocity u and the speed of sound of the flow a as

$$\begin{aligned} c_{+,\,\mathrm{a}} &= u_{\mathrm{a}} + a_{\mathrm{a}}, \\ c_{+,\,\mathrm{b}} &= u_{\mathrm{b}} + a_{\mathrm{b}}. \end{aligned} \tag{11}$$

Using Eqs (9)–(11), we can estimate the shock reformation distance after the weak shock wave becomes compression waves with the thickness of Δx. With the determined values of u_{a} and a_{a}, the values of u_{b} and a_{b} can be calculated using the isentropic relationship for a given pressure jump. Because properties changed by weak shock wave can be regarded as isentropic, the pressure jump across compression waves is regarded the same as that across the weak shock wave. Thus, $L/\Delta x$ can be calculated for a given shock Mach number M_{s}, as shown in Figure 8. We use the value of $u_{\mathrm{a}} = -340$ m/s and $a_{\mathrm{a}} = 478$ m/s, which are the same conditions as those in the experiment. The value of $L/\Delta x$ decreases with increases in M_{s}. This is because $c_{+,\,\mathrm{b}}$ becomes large for a strong compression waves. This tendency indicates that the weak shock wave requires a longer shock formation distance than the strong shock does. The value of $L/\Delta x$ is 23 for $M_{\mathrm{s,L\text{-}tSW}} = 1.006$. This calculation indicates that if the shock wave of $M_{\mathrm{s,L\text{-}tSW}} = 1.006$ transforms into compression waves of thicknesses equivalent to the integral scale of the turbulence, a propagation length of approximately ten times the order of the integral scale is needed to recover the shock profile. On the contrary, the shock waves of $M_{\mathrm{s,L\text{-}tSW}} = 1.034$ and 1.046 require propagation distances of 4.3 and 3.2 times Δx, respectively. In these relatively strong shock wave cases, it is possible that the local compression waves soon reform as the shock wave. Therefore, the assumption that the vanished parts of the shock wave are not recovered during the interaction is appropriate for very weak shock waves, such as those satisfying $L/\Delta x \geq O(10^1)$. For

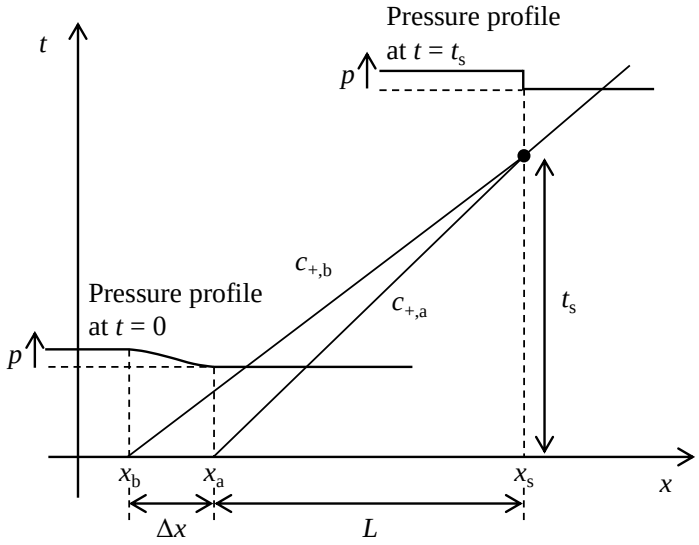

Figure 7: Schematic of shock formation by the integration of compression waves, as presented by Sasoh (2020).

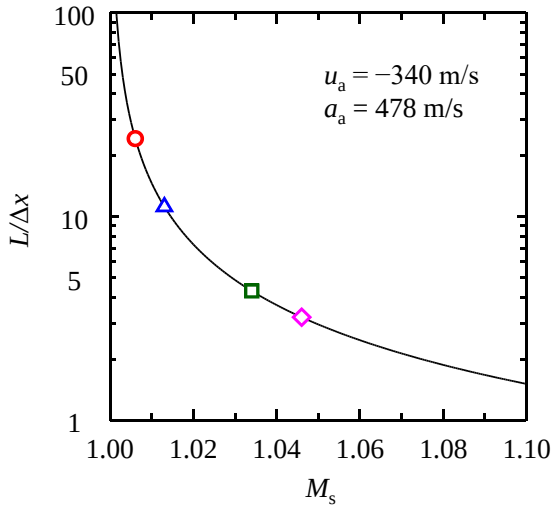

Figure 8: Ratio of shock formation distance to thickness of compression wave $L/\Delta x$ as a function of M_s. Plots correspond to the shock Mach numbers examined in the experiment.

simplicity, we assume that the shock waves of $M_{\mathrm{s,L\text{-}tSW}} = 1.006$ and 1.013 do not recover once they experience discontinuous profile loss.

Based on the above discussions, the vanishment of weak shock waves $M_{\mathrm{s,L\text{-}tSW}} = 1.006$ and 1.013 is modeled by considering the interaction length effect. In a repetitive interaction with the velocity fluctuation, we define the probability of

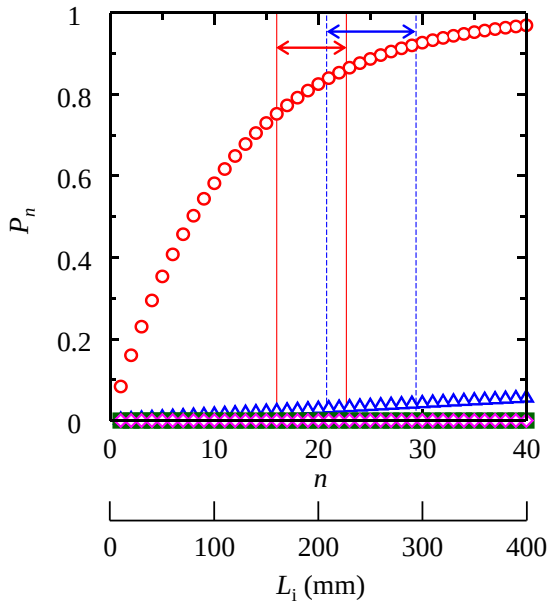

Figure 9: Shock vanishment probability in n interactions with the velocity fluctuation. The interaction length for the integral scale of 10 mm is also shown in the horizontal axis. $\widetilde{M}_\mathrm{t} = 0.025$ under all conditions and $M_\mathrm{s,L\text{-}tSW} = 1.006$ (circle), $M_\mathrm{s,L\text{-}tSW} = 1.013$ (triangle), $M_\mathrm{s,L\text{-}tSW} = 1.034$ (square), and $M_\mathrm{s,L\text{-}tSW} = 1.046$ (diamond). Regions indicated by a double arrow correspond to L_i where in the present experiment the shock wave front profile vanishes judged from the schlieren images at $M_\mathrm{s,L\text{-}tSW} = 1.006$ (solid line) and $M_\mathrm{s,L\text{-}tSW} = 1.013$ (dashed line).

local shock wave vanishment over n interactions as P_n. In $n+1$ interactions, P_{n+1} is expressed as the sum of the following independent cases: one is that the local shock wave remains after n interactions and then vanishes after $n+1$ interactions, and the other is that the local shock wave has already vanished during interactions 1 to n. The probability of the former is $P\left(m_x > M_\mathrm{R}\right)(1 - P_n)$ by considering the conditional probability, and that of the latter is P_n. Therefore, we obtain Pn+1 in the recurrence formula as $P_{n+1} = P\left(m_x > M_\mathrm{R}\right)(1 - P_n) + P_n$. Here, the first term of P_n satisfies the relationship of $P_1 = P\left(m_x > M_\mathrm{R}\right)$ as shown in Eq(7). The general term of P_n can be derived in the form of a geometric progression as

$$P_n = 1 - \left[1 - P\left(m_x > M_\mathrm{R}\right)\right]^n . \tag{12}$$

Meanwhile, for the relatively strong shock waves with $M_\mathrm{s,L\text{-}tSW} = 1.034$ and 1.046, we can regard P_n as approximately 0 because the shock wave vanishment criterion Eq(8) is not satisfied, as seen in Figure 6, and the shock wave is soon reformed from the profile of the compression waves, as seen in Figure 8.

The phenomenon of gradual shock wave vanishment with increasing interaction length observed in the experiment is physically considered using the developed model. We can assume that the integral length scale of turbulence represents the length of

one velocity fluctuation, because the integral scale of turbulence physically corresponds to the length of the dominant scale of eddies in turbulent flow. In the previous measurement of grid turbulence in the CD-ST, the integral scale of grid turbulence was approximately 10 mm for the turbulence mean flow of 50–160 m/s (Fukushima et al 2021). In the present research, we adopted this value as the integral scale of grid turbulence. Therefore, the interaction length consumed by one interaction with the velocity fluctuation is 10 mm in this model. In the experiment results, because the largest value of the interaction length was approximately 300 mm, we visualized an interaction length of 30 times that of the shock wave with the velocity fluctuation in this study. The value of P_n is plotted as a function of the number of interactions n in Figure 9. The interaction length L_i for the integral scale of 10 mm is also shown in the horizontal axis. Four kinds of plots correspond to the experimental conditions. With an increase in L_i, P_n sharply increased in the case of the weakest shock Mach number of $M_{\mathrm{s,L\text{-}tSW}} = 1.006$. The vanishment probability exceeds 80% for $L_\mathrm{i} = 200$ mm. The calculation from this model is consistent with the experimental results of decreasing the side-view projected shock wave contrast with increasing interaction length. The model shows good agreement with the experimental results of total shock wave vanishment at approximately $L_\mathrm{i} = 200$ mm. Furthermore, in the cases of relatively strong shock waves of $M_{\mathrm{s,L\text{-}tSW}} = 1.034$ and 1.046, the shock wave vanishment probabilities remain near zero. The proposed shock wave vanishment model is also consistent with the experimental results of a totally continuous shock wave profile on the side-view image. However, on the border condition $M_{\mathrm{s,L\text{-}tSW}} = 1.013$, the model cannot quantitatively describe the experimental results. The model shows 4% vanishment on a shock wave profile at $L_\mathrm{i} = 300$ mm, while the experiment showed widely shock wave vanishment at approximately $L_\mathrm{i} = 300$ mm.

According to the comparison of the experimental results, a precise agreement is not achieved around the condition where the shock Mach number and the turbulent Mach number begin to satisfy the shock wave vanishment criteria $\left(M_{\mathrm{s,L\text{-}tSW}} = 1.013, \widetilde{M_\mathrm{t}} = 0.025\right)$. On the contrary, the proposed shock wave vanishment model based on the solution of the 1D unsteady compression problem can explain the weak shock wave vanishment in the interaction length range of 10 times the order of the integral scale of grid turbulence.

5. Conclusion

In this study, the losing the shock wave front profile during interactions with turbulence was investigated experimentally and theoretically. We experimentally demonstrated the vanishment of a weak shock wave profile during interactions with grid turbulence using the CD-ST. On the side projected schlieren images, the contrast of the weak shock wave was gradually decreased with increases in the interaction length. This vanishment was modeled based on a 1D unsteady interaction theory (the Riemann problem). In the 1D interaction of the shock wave with a velocity fluctuation, the shock wave transforms to

a sound wave and even to expansion waves. We expanded the theory to a shock wave interaction with a planar distributed velocity fluctuation. The starting condition for shock wave vanishment was statistically obtained as $M_\mathrm{t} \geq \left({M_\mathrm{s}}^2 - 1\right)/M_\mathrm{s}$ where M_s is the shock Mach number and M_t is the turbulent Mach number. The interaction length effect in the experiment was considered in the proposed shock wave vanishment model by considering a repetitive interaction with the velocity fluctuation. From a quantitative analysis of the characteristic propagation, in the measured interaction range we found that the weak shock wave does not recover once it experiences discontinuous profile loss. Although a precise agreement was not confirmed for conditions where the shock Mach number and the turbulent Mach number begin to satisfy the shock wave vanishment criteria, we confirmed the validity of the proposed model for the vanishment of weak shock waves at interaction lengths of 10 times the order of the integral scale of grid turbulence. The results of this study are expected to help with further understanding of the unsteady shock wave behavior in shock–turbulence interactions. In addition, we believe the knowledge obtained in this study could be valuable for the validation of numerical simulation data as well as for applications in aerospace engineering, such as advancing the understanding of sonic boom modulation by atmospheric turbulence.

Acknowledgments

The authors acknowledge the kind donation of the cellophane diaphragm by Futamura Chemical Co., Ltd. We are grateful for the helpful comments and discussions from Professor K. Nagata, Associate Professor K. Kinefuchi, Assistant Professor T. Watanabe, and Mr. K. Tanaka (Nagoya University). We also thank the valuable technical assistance of the Technical Division of Nagoya University. This research was supported by the JSPS KAKENHI Grants Nos. 17J10997 and 18H03813.

References

Agui J H, Briassulis G and Andreopoulos Y 2005 *J. Fluid Mech.* **524** 143-195 https://doi.org/10.1017/S0022112004002514143-195

Andreopoulos Y, Agui J H, and Briassulis G 2000 *Annu. Rev. Fluid Mech.* **32** 309-345 https://doi.org/10.1146/annurev.fluid.32.1.309

Briassulis G, Agui J, Watkins C B and Andreopoulos Y 1998 *NASA/CR-1998-206948*

Chen C H and Donzis D A 2019 *J. Fluid Mech.* **870** 813-847 https://doi.org/10.1017/jfm.2019.248

Donzis D A 2012 *Phys. Fluids* **24** 126101 https://doi.org/10.1063/1.4772064

Dosanjh D S 1956 *NACA Report* **TN-3680**

Fukushima G, Ogawa S, Wei J, Nakamura Y and Sasoh A *Shock Waves* (Under review)

Glass Irvine I and Sislian J P 1994 *Clarendon Press, Oxford*

Honkan A and Andreopoulos J 1992 *Phys. Fluids A: Fluid Dyn.* **4** 2562-2572 https://doi.org/10.1063/1.858443

Honkan A, Watkins C B and Andreopoulos J 1994 *J. Fluid Eng.* **116** 763-769 https://doi.org/10.1115/1.2911847

Inokuma K, Watanabe T, Nagata K, Sasoh A and Sakai Y 2017 *Phys. Fluids* **29**051701 https://doi.org/10.1063/1.4982932

Inokuma K, Watanabe T, Nagata K and Sakai Y 2019 *Phys. Fluids* **31** 085119 https://doi.org/10.1063/1.5110185

Kim J -H, Sasoh A and Matsuda A 2010 *Shock Waves* **20** 339-345 https://doi.org/10.1007/s00193-010-0265-z

Kitamura T, Nagata K, Sakai Y, Sasoh A and Ito Y 2017 *Phys. Fluids* **29** 065114 https://doi.org/10.1063/1.4984835

Larsson J and Lele S K 2009 *Phys. Fluids* **21** 126101 https://doi.org/10.1063/1.3275856

Larsson J, Bermejo-Moreno I and Lele S K 2013 *J. Fluid Mech.* **717** 293-321 https://doi.org/10.1017/jfm.2012.573

Lee S, Lele S K, Moin P 1993 *J. Fluid Mech.* **251** 533-562 https://doi.org/10.1017/S0022112093003519

Lele S K 1992 *Phys. Fluids* **4** 2900-2905 https://doi.org/10.1063/1.858343

Liepmann H W and Roshko A 1957 *John Wiley & Sons*

Lipkens B and Blackstock D T 1998 *J. Acoust. Soc. Am.* **103** 148-158 https://doi.org/10.1121/1.421114

Livescu D and Ryu J 2016 *Shock Waves* **26** 241-251 https://doi.org/10.1007/s00193-015-0580-5

Monin A S and Yaglom A M 1975 *MIT Press*

Ryu J and Livescu D 2014 *J. Fluid Mech.* **756** R1 https://doi.org/10.1017/jfm.2014.477

Sasoh A, Harasaki T, Kitamura T, Takagi D, Ito S, Matsuda A, Nagata K and Sakai Y 2014 *Shock Waves* **24** 489-500 https://doi.org/10.1007/s00193-014-0507-6

Sasoh A 2020 *Springer Singapore*

Shapiro A H 1953 *The Ronald Press Company*

Tamba T, Furukawa D, Aoki Y, Kayumi M, Iwakawa A, Sasoh A, Matsunaga T, Izumo M, Sugiyama Y, Matsumura T and Nakayama Y 2016 it Sci. Tech. Energetic Materials **77** 91

Tamba T, Nguyen T M, Takeya K, Harasaki T, Iwakawa A and Sasoh A 2015 *Shock Waves* **25** 667-674 https://doi.org/10.1007/s00193-015-0594-z

Tamba T, Fukushima G, Kayumi M, Iwakawa A and Sasoh A 2019 *Phys. Rev. Fluids* **4** 073401 https://doi.org/10.1103/PhysRevFluids.4.073401

Tanaka K, Watanabe T, Nagata K, Sasoh A, Sakai Y and Hayase T 2018 *Phys. Fluids* **30** 035105 https://doi.org/10.1063/1.5019867

Tanaka K, Watanabe T and Nagata K 2020 *Phys. Fluids* **32** 096107 https://doi.org/10.1063/5.0019784

Tian Y, Jaberi F A, Li Z and Livescu D 2017 *J. Fluid Mech.* **829** 551-588 https://doi.org/10.1017/jfm.2017.542

Xanthos S, Briassulis G and Andreopoulos Y 2002 *J. Propul. Power* **18** 1289-1297 https://doi.org/10.2514/2.6066